

Gyroscopic Precession in Axisymmetric Kerr Spacetime: Horizon Regularity and Coordinate Effects

Paulami Majumder¹

Email: pm18rs040@iiserkol.ac.in

¹Centre of Excellence in Space Sciences India (CESSI),
Indian Institute of Science Education and Research Kolkata,
Mohanpur, West Bengal 741246, India

Abstract

We investigate gyroscopic precession along Killing and non-Killing timelike trajectories in Kerr spacetime using the covariant Frenet–Serret formalism. The precession frequency is analyzed for both prograde and retrograde motion in Boyer–Lindquist and horizon-penetrating Kerr–Schild coordinate systems. For generic spiral trajectories, we show explicitly that the divergence of the precession frequency appearing near the horizon in Boyer–Lindquist coordinates disappears in Kerr–Schild coordinates. Our analysis demonstrates that the finiteness of the Frenet–Serret precession frequency is determined by the timelike character of the trajectory rather than by the existence of an event horizon itself. These results indicate that the divergence of gyroscopic precession in the strong-field regime is a coordinate artefact and therefore cannot serve as an invariant signature of horizon structure.

Keywords: Kerr spacetime, Gyroscopic Precession, Frenet–Serret Formalism, Frame Dragging, Kerr–Schild coordinates, Black Hole physics

1 Introduction

Gyroscopic precession in rotating spacetimes provides an important probe of frame dragging and strong-field gravitational dynamics in general relativity. In Kerr spacetime, the spin evolution of a test gyroscope encodes the coupling between orbital motion and spacetime rotation, making gyroscopic precession a useful diagnostic of relativistic spin transport near compact objects.

The study of relativistic spin precession dates back to the works of Lense, Thirring, and Schiff [1, 2, 3], and received direct experimental confirmation through the Gravity Probe B mission [4]. In stationary and axisymmetric spacetimes, gyroscopic precession has been extensively investigated using both kinematical and geometrical approaches [5, 6]. In particular, the covariant Frenet–Serret (FS) formalism developed in Refs. [7, 8, 9, 10, 11] provides a natural geometric framework for describing spin precession along accelerated worldlines in curved spacetime.

Most previous analyses in Kerr geometry have focused primarily on Killing observers and circular equatorial motion. However, realistic strong-gravity trajectories are generally non-geodesic and non-Killing. In astrophysical inspirals, radiation reaction and

self-force effects continuously drive the motion away from exact circularity, particularly in extreme mass-ratio inspirals (EMRIs) [12]. Spin precession also plays an important role in compact-binary dynamics and gravitational-wave observations, where spin-orbit coupling leaves characteristic imprints on the emitted waveform [13, 14, 15, 16, 17, 18, 19]. Extreme mass-ratio inspirals detectable by the future Laser Interferometer Space Antenna (LISA) are expected to provide precision probes of strong-field Kerr geometry and possible deviations from the black-hole paradigm through long-duration relativistic inspirals [20, 21]. These developments motivate the study of gyroscopic precession along more general timelike trajectories in rotating spacetimes.

An important issue concerns the behaviour of gyroscopic precession close to the event horizon. In Boyer–Lindquist coordinates, the precession frequency is often found to diverge near the horizon and has sometimes been interpreted as a physical signature of strong gravity. Nevertheless, recent studies in Schwarzschild and Reissner–Nordström spacetimes [22, 23] have shown that such divergences arise from coordinate singularities rather than invariant physical effects. This indicates that the behaviour of gyroscopic precession in the strong-field regime must be analyzed using fully covariant methods together with horizon-regular coordinate systems.

The problem is also relevant in the broader context of distinguishing black holes from horizonless compact objects and naked singularities. Since naked singularities violate the cosmic censorship conjecture [24], identifying invariant strong-gravity diagnostics capable of differentiating horizon geometries remains an active area of research. Previous investigations suggested that gyroscopic precession may provide possible observational distinctions between black holes and naked singularities [23]. However, the behaviour of gyroscopic precession along generic timelike trajectories in Kerr spacetime, particularly in horizon-penetrating coordinate systems, remains comparatively unexplored.

In this work, we investigate gyroscopic precession in Kerr spacetime along both Killing and non-Killing timelike trajectories using the covariant Frenet–Serret formalism. We analyze prograde and retrograde motion in both Boyer–Lindquist and Kerr–Schild coordinate systems. For logarithmic spiral trajectories, we show explicitly that the divergence of the FS precession frequency appearing in Boyer–Lindquist coordinates disappears in horizon-penetrating Kerr–Schild coordinates. Our analysis demonstrates that the finiteness of the precession frequency is governed by the timelike character of the trajectory rather than by the existence of an event horizon itself. Consequently, divergent gyroscopic precession cannot be regarded as a coordinate-invariant diagnostic of horizon structure.

The paper is organized as follows. In Sec. 2, we briefly review the Kerr geometry and the relevant observer structure. In Sec. 3, we study gyroscopic precession along circular Killing trajectories. In Sec. 4, we investigate gyroscopic precession along non-Killing logarithmic spiral trajectories in both Boyer–Lindquist and Kerr–Schild coordinate systems. Finally, we summarize the results and discuss their implications in Sec. 5.

Notations and Conventions

We have used $(+, -, -, -)$ metric signature throughout this paper. We have also used natural units *i.e.*, $G = c = 1$.

2 Brief Overview on Kerr Spacetime

The Kerr spacetime is a stationary, axisymmetric, and asymptotically flat vacuum solution of Einstein’s field equations describing a rotating compact object with mass M and spin

parameter $a = J/M$ [25, 26, 27]. In Boyer–Lindquist coordinates, the metric is given by

$$ds^2 = \left(1 - \frac{2Mr}{\Sigma}\right) dt^2 - \frac{\Sigma}{\Delta} dr^2 - \Sigma d\theta^2 + \frac{4Mra \sin^2 \theta}{\Sigma} d\phi dt - \left(r^2 + a^2 + \frac{2Mra^2 \sin^2 \theta}{\Sigma}\right) \sin^2 \theta d\phi^2, \quad (1)$$

where

$$\Delta = r^2 + a^2 - 2Mr, \quad \Sigma = r^2 + a^2 \cos^2 \theta. \quad (2)$$

The horizons are located at the roots of $\Delta = 0$,

$$r_{\pm}^{EH} = M \pm \sqrt{M^2 - a^2}, \quad (3)$$

while the ergosurfaces are situated at

$$r_{\pm}^{Ergo} = M \pm \sqrt{M^2 - a^2 \cos^2 \theta}. \quad (4)$$

The Kerr geometry admits two commuting Killing vectors associated with stationarity and axial symmetry, namely ξ^a and η^a [6]. Due to frame dragging, static timelike observers cannot exist inside the ergoregion. The corresponding locally non-rotating observers are the zero-angular-momentum observers (ZAMOs), defined through the hypersurface-orthogonal vector

$$\zeta^a = \xi^a - \left(\frac{\xi^b \eta_b}{\eta^c \eta_c}\right) \eta^a. \quad (5)$$

In this work, we investigate gyroscopic precession along both Killing and non-Killing timelike trajectories in Kerr spacetime using the covariant Frenet–Serret formalism [6]. Particular attention is given to the behaviour of the precession frequency near the horizon in both Boyer–Lindquist and horizon-penetrating Kerr–Schild coordinates, with applications to strong-gravity trajectories relevant for inspiral dynamics and rotating compact objects.

3 Precession of a Gyroscope Along a Killing Trajectory in Kerr Spacetime

The set of circular orbits on the equatorial plane of the Kerr spacetime is represented by the four velocity,

$$u^\mu = \frac{1}{\mathcal{A}} (1, 0, 0, \omega), \quad (6)$$

Where $\mathcal{A}^2 = \left(1 - \frac{2Mr}{\Sigma}\right) + \frac{4Mra}{\Sigma} \omega - \left(r^2 + a^2 + \frac{2Mra^2}{\Sigma}\right) \omega^2$ is the normalizing factor such that the norm of the 4-velocity will be timelike. Here ω need not be constant for the congruences; it is sufficient to have the condition $\mathcal{L}_\xi \omega = 0 = \mathcal{L}_\eta \omega$. The angular speed ω can be decomposed with reference to the fundamental angular speed of the irrotational congruence as $\omega = \tilde{\omega} + \omega_0$, where ω_0 is given by Eq. (5). The timelike condition provides $(g_{tt} + 2\omega g_{t\phi} + \omega^2 g_{\phi\phi}) > 0$ and the real roots of the quadratic equation give the allowed values of the angular velocity ω ,

$$\omega_{\mp} = \frac{-g_{t\phi} \pm \sqrt{(g_{t\phi})^2 - g_{tt}g_{\phi\phi}}}{g_{\phi\phi}}. \quad (7)$$

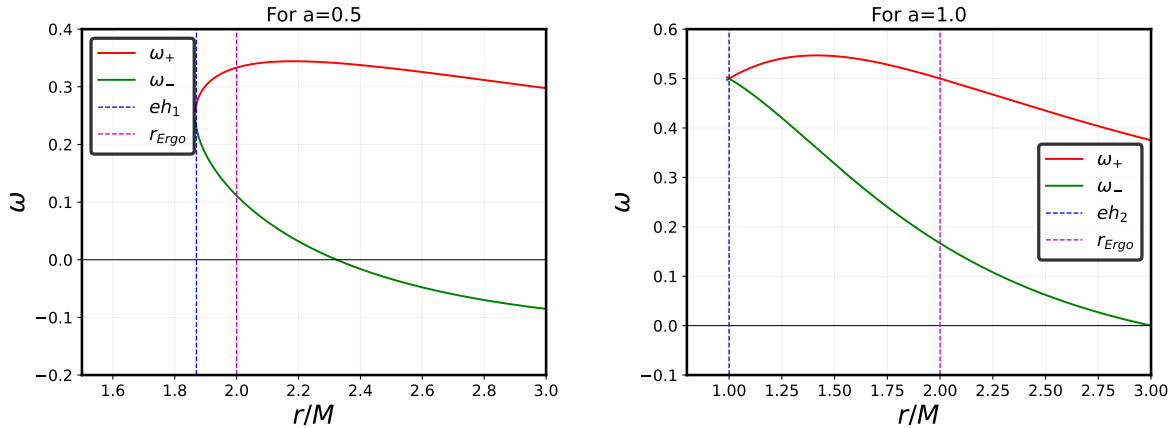


Figure 1: Variation of angular velocity ω_{\pm} given in Eq. (7) as a function of r for different values of black hole spin parameter a .

The difference between the two distinct roots given in Eq. (7) can be evaluated as,

$$\omega_+ - \omega_- = -\frac{2\sqrt{g_{t\phi}^2 - g_{tt}g_{\phi\phi}}}{g_{\phi\phi}}. \quad (8)$$

The discriminator $\sqrt{g_{t\phi}^2 - g_{tt}g_{\phi\phi}}$ of Eq.(8) is positive for real roots. From our usual convention of metric signature, $g_{\phi\phi} < 0$. As a consequence, the difference between the two distinct roots is positive *i.e.*, $\omega_+ > \omega_-$. So the allowed values of ω for a stationary observer must lie between $\omega_- < \omega < \omega_+$. In the next part, we will discuss two types of observers in Kerr spacetime: Co-rotating and Counter-rotating observers with angular velocity ω_+ and ω_- , respectively.

3.1 Precession of Gyroscope for Co-Rotating and Counter-Rotating Trajectories

In Kerr spacetime, depending on the direction of the black hole spin parameter a and the dragging of the inertial frame, both prograde and retrograde orbits are possible. Any stationary observer moving along a timelike trajectory in Kerr spacetime can be either co-rotating or counter-rotating. As the co-rotating observers move in the same direction as the black hole's rotation, the frame-dragging effect reduces the gravitational attraction on them. As a result, this orbit can remain stable much closer to the event horizon. Whereas the counter-rotating observers move in the opposite direction to the rotation of the black hole, they experience a much weaker frame-dragging effect, and they orbit further away from the event horizon. This is also reflected in the radius of the innermost stable circular orbit (ISCO). For an extreme Kerr black hole *i.e.*, for $a = M$, along a geodesic, the ISCO lies at $r = M$ for prograde orbit, followed by the co-rotating observer, and for retrograde orbit, the ISCO radius is pushed out to $r = 9M$ [28]. For co-rotating observer $\omega_+ a > 0$ whereas for counter-rotating observer $\omega_- a < 0$. We will now discuss the possibility of the presence of the co- and counter-rotating observers in some important regions in the Kerr spacetime.

As discussed above, for a stationary observer following a timelike trajectory in Kerr spacetime, the angular velocity of the observer must lie within ω_{\pm} . From Eq. (7), we can write

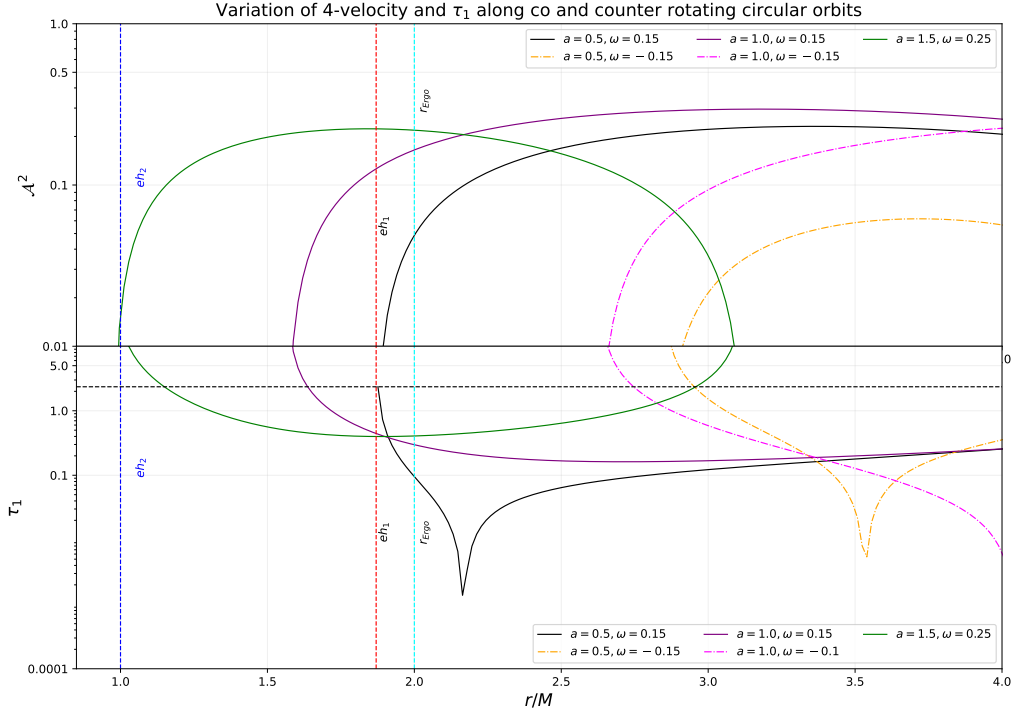


Figure 2: The norm of 4-velocity and FS parameters of co and counter-rotating observer along timelike Killing trajectory in Kerr spacetime in standard coordinate system.

the allowed values of the angular velocity ω on the equatorial plane of the Kerr metric as,

$$\omega_{\mp} = \frac{-g_{t\phi} \pm \sqrt{\Delta}}{g_{\phi\phi}}. \quad (9)$$

Now on the outer horizon *i.e.*, at $r = r_+^{EH}$, $\Delta = 0$. Therefore, on the horizon

$$\omega_{\pm}|_{EH} = \omega_{EH} = -\frac{g_{t\phi}}{g_{\phi\phi}}, \quad (10)$$

ω_{EH} is positive. This is the angular velocity of ZAMO moving on the outer horizon. It is also referred to as the angular velocity of the horizon itself. So on the horizon, only the corotating observer with angular velocity ω_{EH} is allowed.

On the infinite redshift surface $g_{tt} = 0$. From Eq.(7), it is clear on the infinite redshift surface, $\omega_- = 0$, $\omega_+ = -\frac{2g_{t\phi}}{g_{\phi\phi}} > 0$.

Outside of the ergoregion, $g_{tt} > 0$, $g_{\phi\phi} < 0$ and $g_{t\phi} > 0$ and as a consequence, $g_{t\phi}^2 - g_{tt}g_{\phi\phi} > g_{t\phi}^2$. So, it is evident from Eq.(7) that outside of the ergoregion $\omega_+ > 0$ and $\omega_- < 0$. So in that region, both co-rotating and counter-rotating observers are possible. Inside the ergoregion $g_{tt} < 0$, so $g_{t\phi}^2 - g_{tt}g_{\phi\phi} < g_{t\phi}^2$. From Eq.(7) it is clear that, inside the ergoregion, both ω_+ and ω_- are positive. Physically, it indicates that inside the ergoregion, any timelike observer is dragged to co-rotate with the black hole. No counter-rotating observer can exit inside the ergoregion.

For a gyroscope moving along a circular path on the equatorial plane of Kerr spacetime, Eq.(7) can be simplified as,

$$\omega_{\pm}|_{\theta=\frac{\pi}{2}} = \frac{2Mra \pm r\sqrt{\Delta}}{r(r^2 + a^2) + 2Ma^2}. \quad (11)$$

The variations of the allowed values of the angular velocity of circular orbits in Kerr spacetime are plotted as a function of $\frac{r}{M}$ in Fig. 1. For $a = 0.5$, both ω_+ and ω_- approaches to the angular velocity for ZAMO *i.e.*, ω_{EH} . For extremal case *i.e.*, for $a = M$, both roots coincide at the position of the horizon. For the circular Killing orbit, the FS parameters are given by,

$$\begin{aligned}\kappa^2 &= \frac{\frac{\Delta M^2}{r^6} \left[(a\omega - 1)^2 - \frac{r^3 \omega^2}{M} \right]^2}{\left[1 - (r^2 + a^2) \omega^2 - \frac{2m(a\omega - 1)^2}{r} \right]^2}, \\ \tau_1^2 &= \frac{\frac{Ma}{r^2} - \left(\frac{(r^2 + 2a^2)M}{r^2} - r\omega \left(1 - \frac{2M}{r} \right) \right) + \frac{Ma\omega^2(a^2 + 3r^2)^2}{r^2}}{\left[1 - (r^2 + a^2) \omega^2 - \frac{2m(a\omega - 1)^2}{r} \right]^2}, \\ \tau_2^2 &= 0.\end{aligned}\tag{12}$$

In Fig. 2, the variations of the FS parameters for both co-rotating and counter-rotating observers are plotted as a function of $\frac{r}{M}$ for different values of a . From the figure, it is clear that due to the coordinate singularity present at the position of the horizon, the normalized value of the four-velocity becomes null just before the horizon and as a result the precession frequency τ_1 blows up close to the horizon as observed for the static case also [22, 23]. The disappearance of counter-rotating trajectories inside the ergoregion arises naturally from the structure of the allowed angular velocity roots. Within the ergoregion, both roots of ω become positive, enforcing co-rotation with the black hole. This behaviour is reflected in the gyroscopic precession rate, which offers a physical interpretation of the ergoregion as the region where frame dragging becomes so strong that counter-rotation is forbidden. This provides a potential tool for distinguishing between black holes and spinning horizonless compact objects with altered ergoregion structure. In the next section, we apply the generalised FS formalism discussed in [22] to study the precession frequency along a non-Killing spiral trajectory in Kerr spacetime.

4 Gyroscopic Precession along Spiral Trajectory

Apart from the Killing case, one can also study the GP along any arbitrary timelike trajectory, such as a non-Killing trajectory [22]. Since the FS formalism is completely covariant, it can also be used for non-Killing trajectories. Recent studies have also shown that gyroscopic precession (GP) plays a substantial role in the dynamics of extreme-mass-ratio inspirals (EMRIs), which will be key gravitational-wave sources for the upcoming LISA mission. Recent analytical studies of spinning-particle motion in Kerr spacetime have further emphasized the importance of spin transport and spin-orbit coupling effects in strong gravitational fields, particularly for nearly spherical inspiral trajectories and EMRI dynamics [29, 30]. In particular, Destounis et al. [12] report that inspirals into rotating exotic compact objects—such as rotating boson stars—exhibit non-integrability and transient resonances, significantly affecting the precession behaviour of both orbital and spin degrees of freedom. These results deepen the motivation for analysing GP in generic, non-Killing trajectories, as strong-field inspirals rarely follow exact circular equatorial geodesics. We begin our analysis in the standard Boyer–Lindquist coordinate system and subsequently reformulate the discussion in horizon-penetrating Kerr-Schild coordinates.

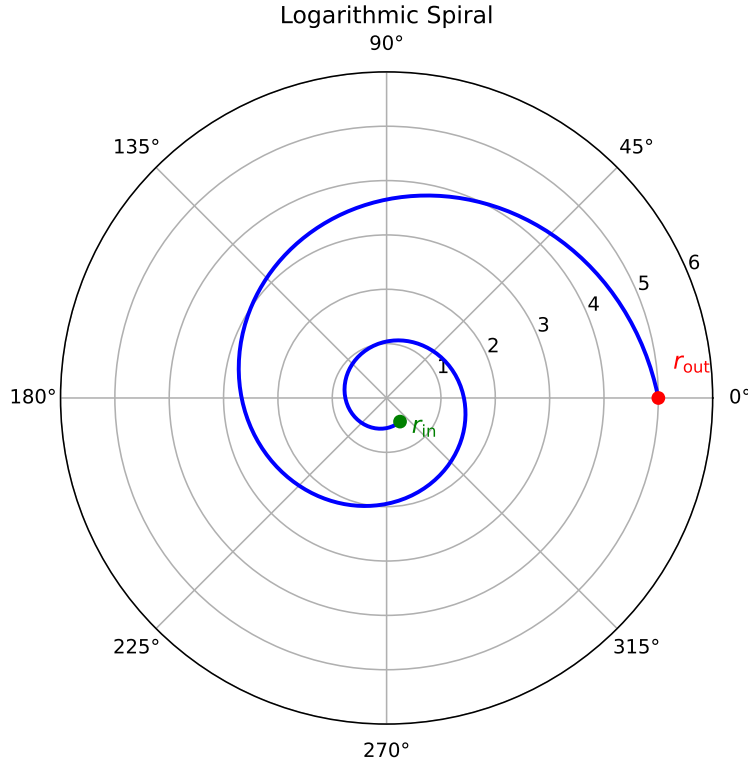


Figure 3: The Logarithmic Spiral $r = r_{out}e^{\lambda\phi}$

4.1 Standard Coordinate System

In this section, we will study the precession frequency of a gyroscope moving along a timelike spiral trajectory in Kerr spacetime. For simplicity, we have used the logarithmic spiral trajectory for our study. Non-Killing logarithmic spiral trajectories provide useful toy models for matter motion in realistic accretion environments. The resulting trajectories naturally include radial velocities, making the study of GP along such paths relevant for interpreting quasi-periodic oscillations (QPOs). In addition, spiral-like inspiral tracks closely resemble the evolution of compact objects in EMRIs, where radiation reaction forces break exact Killing symmetries. Any specific spacetime symmetry does not generate this spiral path, so the gyroscope following this kind of trajectory must have a four-velocity component along the radial and azimuthal directions. Spiral trajectories have the simple relation between r and ϕ which is given by $r = r_{out}e^{\lambda\phi}$. Here the logarithmic spiral starts spiralling from $r = r_{out}$ with the spiral path parameter $\lambda = \frac{1}{2\pi n} \ln\left(\frac{r_{in}}{r_{out}}\right)$, the gyro reaches the radius $r = r_{in}$ after n number of turns in Fig.(3). For a gyroscope moving along a spiral trajectory on the equatorial plane of Kerr spacetime, the four-velocity can be written as,

$$u^a = \frac{1}{\mathcal{B}} (1, r\lambda\omega, 0, \omega), \quad (13)$$

where the normalization factor is defined by,

$$\mathcal{B}^2 = \left(1 - \frac{2Mr}{\Sigma}\right) - \frac{\Sigma}{\Delta} (r\lambda\omega)^2 + 2\omega \frac{2Mra \sin^2 \theta}{\Sigma} - \left(r^2 + a^2 + \frac{2Mra^2 \sin^2 \theta}{\Sigma}\right) \omega^2. \quad (14)$$

Here also, for a timelike trajectory, the normalization factor \mathcal{B}^2 must be positive. This timelike condition restricts the values of the angular velocity ω in the same manner as

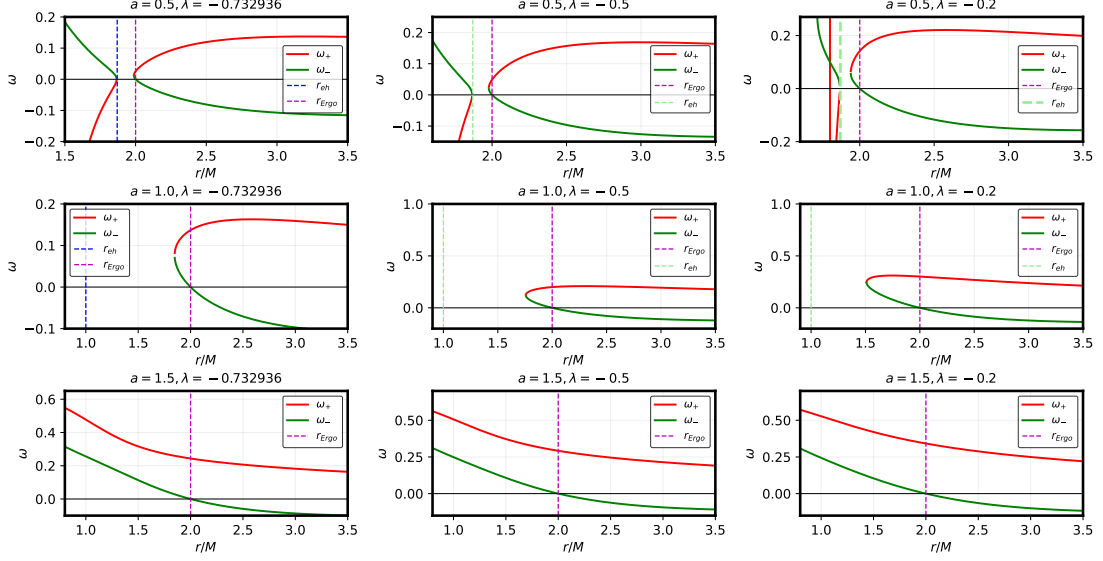


Figure 4: Variation of allowed values of ω vs. $\frac{r}{M}$ along the timelike spiral orbit for different values of black hole spin parameter a and spiral path parameter λ .

the Killing case. The allowed values of ω for the spiral trajectory are given by,

$$\omega_{\mp} = \frac{-g_{t\phi} \pm \sqrt{(g_{t\phi})^2 - (g_{\phi\phi} + g_{rr}r^2\lambda^2)g_{tt}}}{(g_{\phi\phi} + g_{rr}r^2\lambda^2)} \quad (15)$$

Now we can discuss the possibilities of the existence of both co-rotating and counter-rotating observers along this spiral trajectory on some important surfaces of the Kerr spacetime.

On the infinite redshift surface of Kerr spacetime $g_{tt} = 0$. Substituting the value of g_{tt} on equation (15) we get,

$$\omega_{\mp} = \frac{-g_{t\phi} \pm g_{t\phi}}{(g_{\phi\phi} + g_{rr}r^2\lambda^2)}, \quad (16)$$

From the above equation (16), it is evident that $\omega_- = 0$ which corresponds to a static observer and $\omega_+ = \frac{-2g_{t\phi}}{(g_{\phi\phi} + g_{rr}r^2\lambda^2)}$ which is positive due to the choice of our metric signature.

So, no counter-rotating observer is allowed to follow the non-Killing spiral trajectory on the infinite redshift surface.

For the Kerr metric in the standard coordinate system, $g_{rr} = -\frac{\Sigma}{\Delta} \rightarrow \infty$, on the horizon. Near the horizon, the denominator of eq. (15) becomes, $(g_{\phi\phi} + g_{rr}r^2\lambda^2) \approx \frac{\Sigma}{\Delta}r^2\lambda^2 \rightarrow \infty$.

Now on the horizon, since $\Delta \rightarrow 0$, the last term of the discriminant of eq. (15) is more dominating over the others. On the horizon, the discriminant approximately becomes,

$$\sqrt{(g_{t\phi})^2 - (g_{\phi\phi} + g_{rr}r^2\lambda^2)g_{tt}} \approx \sqrt{\frac{\Sigma}{\Delta}r\lambda\sqrt{g_{tt}}}, \quad (17)$$

and it becomes infinite. The two roots of ω will be approximately

$$\omega_{\mp} \approx \pm \frac{\sqrt{\left(\frac{\Sigma}{\Delta}\right)r\lambda\sqrt{g_{tt}}}{\left(\frac{\Sigma}{\Delta}\right)r^2\lambda^2}}, \quad (18)$$

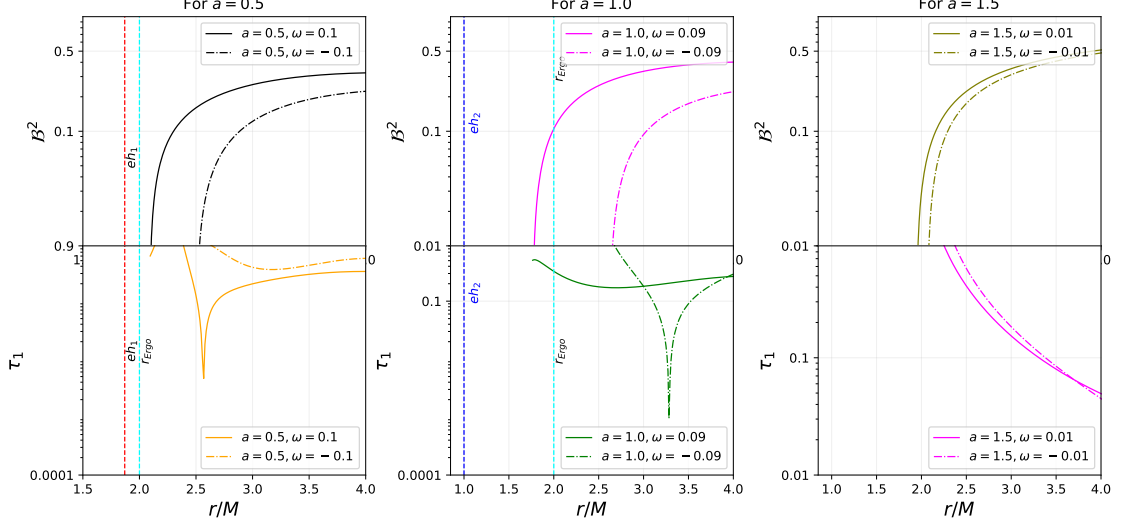


Figure 5: Norm of 4-velocity and FS parameters of co and counter-rotating gyroscope along timelike spiral trajectory in Kerr spacetime in standard coordinate system.

which is proportional to $\sqrt{\left(\frac{\Delta}{\Sigma}\right) g_{tt}}$. Although the discriminant and the denominator of eq. (15) both diverge close to the horizon, the ratio structure of ω_{\mp} regularises it. On the horizon $\omega_{\mp} \rightarrow 0$ as $\Delta \rightarrow 0$. This behaviour differs qualitatively from the Killing case. For the Killing case, the allowed value of ω on the horizon tends to the ZAMO angular velocity $\omega_{EH} = -\frac{g_{t\phi}}{g_{\phi\phi}}$, but for the non-Killing trajectory it tends to zero on the horizon, which can be seen clearly from Fig. 4.

Inside the Ergoregion $g_{tt} < 0$, and the discriminant must be positive for real roots. This implies that within the ergoregion, all observers must co-rotate with the black hole; no counter-rotating observer can physically exist inside this region. The variations of the allowed values of ω as a function of r with different values of λ and a are shown in Fig. 4. From this figure, it is clear that due to the nonvanishing term $g_{rr}r^2\lambda^2$, the roots of the Eq. 15 are different from the Killing one. Logarithmic spiral trajectories, which include both radial and azimuthal motion, exhibit qualitatively different behaviour from Killing circular orbits. In particular, the allowed angular velocity tends to zero at the horizon, naturally regularising the precession frequency. This contrasts sharply with the Killing observers, whose angular velocity must approach the horizon angular velocity ω_{EH} . This result demonstrates that realistic inspiral paths, such as those relevant for extreme mass ratio inspirals (EMRIs), do not exhibit pathological or divergent spin evolution near the horizon. Hence, non-Killing motion captures a more physically meaningful picture of gyroscopic behaviour in strong gravitational fields.

For a gyroscope moving along the timelike spiral trajectory on the equatorial plane of

Kerr spacetime, the normalized four-velocity and FS scalars are given by,

$$\begin{aligned} \kappa^2 = & - \left(a^2 + \frac{2a^2m}{r} + r^2 \right) \mathcal{P}_K^2 - \frac{4am}{r} \mathcal{P}_K \mathcal{Q}_K \\ & - \left(1 - \frac{2m}{r} \right) \mathcal{Q}_K^2 + \frac{r^2}{\Delta} \Xi(r), \end{aligned} \quad (19)$$

$$\dot{\kappa} = \frac{\mathcal{B}_K(r)}{2\kappa} \Pi'(r),$$

$$\tau_1^2 = \frac{1}{\kappa^2} \left(\kappa^4 - \dot{\kappa}^2 + \frac{r^2}{\Delta} \mathcal{H}^0 \right) - \left(a^2 + \frac{2a^2m}{r} + r^2 \right) (\mathcal{H}^1)^2 \quad (20)$$

$$- \frac{4am}{r} \mathcal{H}^1 \mathcal{H}^2 - \left(1 - \frac{2m}{r} \right) (\mathcal{H}^2)^2. \quad (21)$$

where the exact expressions of \mathcal{P}_K , \mathcal{Q}_K , Ξ , \mathcal{B}_K , \mathcal{H}^a , Π are given in [Appendix A](#).

For a gyroscope moving along the timelike spiral trajectory on the equatorial plane of Kerr spacetime, the normalized four-velocity \mathcal{B}^2 and precession frequency τ_1 are plotted as a function of $\frac{r}{M}$ for different values of the Kerr parameter a , angular velocity ω for co and counter-rotating observer and spiral path parameter λ in figure (5). Due to the coordinate singularity at the position of the event horizon, the timelike orbits become null close to the horizon. To eliminate coordinate artefacts near the horizon, we transform our coordinates into a horizon-penetrating Kerr-Schild coordinate system and study the GP near the horizon. In the next section, we will discuss this in more detail.

4.2 Kerr-Schild Coordinate System

The coordinate singularity at the horizon can be removed by a coordinate transformation to a horizon-penetrating Kerr-Schild coordinate system (t', r, θ, ϕ')

$$\begin{aligned} dt' &= dt + \frac{2Mr}{\Delta} dr, \\ d\phi' &= d\phi + \frac{a}{\Delta} dr. \end{aligned} \quad (22)$$

In this coordinate system, the Kerr metric can be written as,

$$\begin{aligned} ds^2 = & \left(1 - \frac{2Mr}{\Sigma} \right) (dt')^2 + \frac{4Mar}{\Sigma} \sin^2 \theta dt' d\phi' - \frac{4Mr}{\Sigma} dt' dr \\ & + 2a \sin^2 \theta \left(1 + \frac{2Mr}{\Sigma} \right) dr d\phi' - \left(1 + \frac{2Mr}{\Sigma} \right) dr^2 \\ & - \Sigma d\theta^2 - \frac{((r^2 + a^2)^2 - a^2 \Delta \sin^2 \theta) \sin^2 \theta}{\Sigma} (d\phi')^2. \end{aligned} \quad (23)$$

The four-velocity along the spiral trajectory in the Kerr-Schild coordinate system becomes,

$$u^a = \frac{1}{\mathcal{V}} (1, r\lambda\omega, 0, \omega), \quad (24)$$

where the normalization factor \mathcal{V} is,

$$\begin{aligned} \mathcal{V}^2 = & \left(1 - \frac{2Mr}{\Sigma} \right) - \frac{4Mr}{\Sigma} r\lambda\omega + \frac{4Mar}{\Sigma} \omega - \left(1 + \frac{2Mr}{\Sigma} \right) (r\lambda\omega)^2 \\ & + 2a \left(1 + \frac{2Mr}{\Sigma} \right) r\lambda\omega^2 - \frac{((r^2 + a^2)^2 - a^2 \Delta)}{\Sigma} \omega^2. \end{aligned} \quad (25)$$

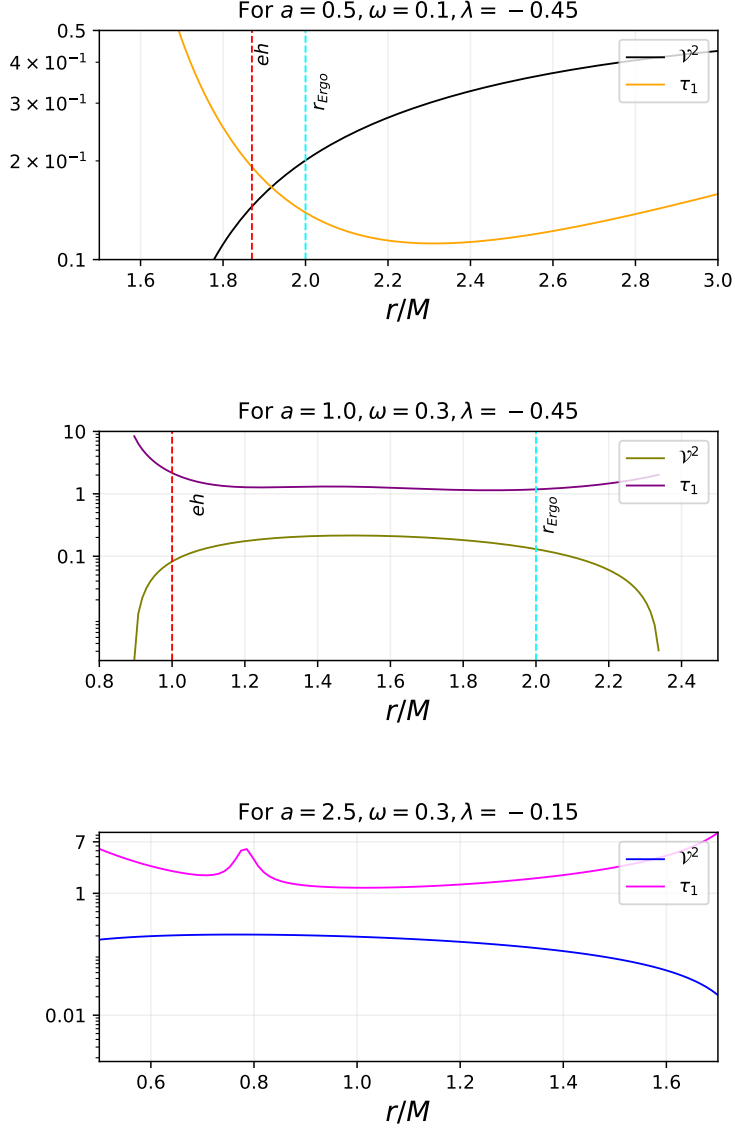


Figure 6: The norm of the 4-velocity and FS parameters of co and counter-rotating gyroscope along timelike spiral trajectory in Kerr spacetime in Kerr-Schild coordinate system.

The FS parameters along a timelike spiral trajectory in Kerr spacetime can be expressed in the Kerr-Schild coordinate system in a more compact form as,

$$\begin{aligned}\kappa^2 &= -\Delta_r (\mathcal{R}^3)^2 - \frac{4am}{r} \mathcal{R}^3 \mathcal{R}^1 + \frac{4m}{r} \mathcal{R}^3 \mathcal{R}^2 + \left(1 + \frac{2m}{r}\right) (\mathcal{R}^2)^2, \\ \tau_1^2 &= \frac{1}{\kappa^2} \left[\kappa^4 - \dot{\kappa}^2 - \Delta_r (B^0)^2 - \frac{4am}{r} B^0 B^1 + \frac{4m}{r} B^0 B^2 - \left(1 + \frac{2m}{r}\right) (B^2)^2 \right].\end{aligned}$$

where, the explicit expressions of the parameters \mathcal{R}^a, B^a 's are written in Appendix [Appendix A](#). The normalized four-velocity and τ_1 are plotted as a function of $\frac{r}{M}$ for different values of black hole spin parameter a , the spiral path parameter λ and the angular velocity ω . Since inside the ergoregion the timelike Killing vector becomes spacelike, no counter-rotating observers are allowed, we are considering only the co-rotating orbits with $\omega > 0$ in the strong gravity regime.

Horizon-penetrating Kerr-Schild coordinates are widely used in numerical relativity and black-hole simulations due to their regularity at the horizon and improved behaviour for

strong-field evolution problems [31, 32, 33]. Recent simulations of precessing BBHs in horizon-penetrating coordinates [14, 16] have emphasised the necessity of horizon-regular variables when extracting strong-field signatures, including GP. From fig. 6, it is clear that in the Kerr-Schild coordinate system the precession frequency is finite when the trajectory crosses the horizon for both black hole and naked singularity. This demonstrates that the precession frequency need not diverge near the horizon. The precession frequency remains finite as long as the trajectory remains timelike. So, the divergence of GP frequency in the strong gravity regime cannot be taken as evidence of the existence of an event horizon. The finite behaviour of FS precession frequency seen in our analysis is consistent with these modern numerical insights, reaffirming that divergence in Boyer-Lindquist coordinates is a coordinate artefact rather than a physical effect.

5 Discussion

In this work, we investigated gyroscopic precession (GP) in Kerr spacetime for both Killing and non-Killing timelike trajectories using the covariant Frenet-Serret formalism. The behavior of the allowed angular velocities for co-rotating and counter-rotating observers was analyzed in both Boyer-Lindquist and Kerr-Schild coordinate systems. For circular Killing trajectories, the allowed angular velocity approaches the horizon angular velocity near the event horizon, whereas for non-Killing logarithmic spiral trajectories the angular velocity tends to zero close to the horizon. The structure of the allowed angular velocity roots also reproduces the absence of counter-rotating timelike trajectories inside the ergoregion.

Our analysis demonstrates that the divergence of the FS precession frequency observed near the horizon in Boyer-Lindquist coordinates originates from the coordinate singularity of the spacetime foliation rather than from an invariant physical effect. In horizon-penetrating Kerr-Schild coordinates, the FS precession frequency remains finite for timelike spiral trajectories crossing the horizon. This shows that the regularity of gyroscopic precession is governed primarily by the timelike nature of the trajectory rather than by the existence of an event horizon itself.

These results have important implications for the interpretation of gyroscopic precession as a probe of strong-field gravity. In particular, the divergence of the precession frequency in Boyer-Lindquist coordinates cannot be regarded as a coordinate-invariant signature of horizon structure. More generally, our analysis supports the viewpoint that physically meaningful observables in the strong-gravity regime should be formulated using covariant or horizon-regular quantities.

The present study is also relevant in the context of extreme mass-ratio inspirals (EMRIs), where radiation reaction and self-force effects continuously drive the smaller compact object away from exact Killing trajectories. In realistic EMRI systems, the orbital evolution near a rotating black hole generically involves inspiraling motion with both radial and azimuthal components. Since gyroscopic precession contributes to the evolution of spin and orbital angular momentum, understanding its behavior along non-Killing timelike trajectories is important for modeling relativistic spin dynamics in the strong-field regime. The finite behavior of the FS precession frequency in Kerr-Schild coordinates therefore suggests that horizon-regular formulations may provide a more physically consistent framework for describing spin transport and precession effects in EMRI dynamics.

Our results further indicate that gyroscopic precession may still provide useful information for distinguishing black holes from naked singularities or other exotic compact objects, provided that the analysis is performed in horizon-regular coordinate systems. In this context, the structure of the ergoregion and the behavior of non-Killing trajectories

may offer additional insights into strong-field gravitational dynamics beyond the standard Kerr black hole scenario.

Several extensions of the present work remain open for future investigation. An important next step would be to analyze gyroscopic precession along generic non-equatorial inspiraling trajectories in Kerr spacetime, including the effects of radiation reaction and gravitational self-force corrections relevant for EMRI evolution. It would also be interesting to investigate FS precession in dynamical or modified-gravity black hole spacetimes, where deviations from Kerr geometry could alter the strong-field behaviour of spin transport. Another promising direction is to explore observational imprints of gyroscopic precession in gravitational-wave signals and in horizon-scale astrophysical phenomena.

Acknowledgment

The author is indebted to Prof. Rajesh Kumble Nayak for many useful discussions on the present topic and for also suggesting helpful corrections to the manuscript. The author is also thankful to the Centre of Excellence in Space Sciences India (CESSI), IISER Kolkata.

Data Availability

The work is mainly analytical, so there is no associated data with this manuscript.

Appendix A Compact Expressions for Frenet–Serret Scalars

In this appendix we present compact expressions for the Frenet–Serret (FS) curvature scalar κ , its evolution $\dot{\kappa}$, and the first FS torsion τ_1 for logarithmic spiral trajectories in Kerr spacetime. Lengthy algebraic expressions and intermediate derivations are relegated to the supplementary material.

Appendix A.1 Boyer–Lindquist Coordinates

We define

$$\Delta(r) \equiv r^2 - 2mr + a^2, \quad (\text{A1})$$

$$\mathcal{F}_K(r) \equiv 1 - \frac{2m}{r} + \frac{4am\omega}{r} + \left(-a^2 - \frac{2a^2m}{r} - r^2\right)\omega^2 - \frac{\lambda^2 r^4 \omega^2}{\Delta(r)}. \quad (\text{A2})$$

The auxiliary functions are

$$\mathcal{P}_K(r) \equiv -\frac{\lambda r \omega^2 \mathcal{F}'_K}{2\mathcal{F}_K^2} + \frac{2a\lambda m \omega}{r\Delta\mathcal{F}_K} + \frac{2\lambda(-a^2mr^2 + r^4(-2m+r))\omega^2}{r^3\Delta\mathcal{F}_K}, \quad (\text{A3})$$

$$\mathcal{Q}_K(r) \equiv -\frac{\lambda r \omega \mathcal{F}'_K}{2\mathcal{F}_K^2} + \frac{2\lambda m(a^2 + r^2)\omega}{r\Delta\mathcal{F}_K} - \frac{2a\lambda m(a^2 + 3r^2)\omega^2}{r\Delta\mathcal{F}_K}, \quad (\text{A4})$$

$$\begin{aligned} \Xi(r) \equiv & \frac{m\Delta}{r^4\mathcal{F}_K} - \frac{2am\Delta\omega}{r^4\mathcal{F}_K} + \frac{\lambda^2 r(a^2 - mr)\omega^2}{\Delta\mathcal{F}_K} \\ & - \frac{(-a^2mr^2 + r^5)\Delta\omega^2}{r^6\mathcal{F}_K} + (\mathcal{B}'_K)^2, \end{aligned} \quad (\text{A5})$$

where

$$\mathcal{B}_K(r) \equiv \frac{\lambda r \omega}{\sqrt{\mathcal{F}_K}}. \quad (\text{A6})$$

The FS curvature scalar is

$$\kappa = \left[-\left(a^2 + \frac{2a^2m}{r} + r^2\right)\mathcal{P}_K^2 - \frac{4am}{r}\mathcal{P}_K\mathcal{Q}_K - \left(1 - \frac{2m}{r}\right)\mathcal{Q}_K^2 + \frac{r^2}{\Delta}\Xi(r) \right]^{1/2}. \quad (\text{A7})$$

Defining

$$\Pi(r) \equiv \kappa^2, \quad (\text{A8})$$

the evolution of κ along the trajectory is

$$\dot{\kappa} = \frac{\mathcal{B}_K(r)}{2\kappa} \Pi'(r). \quad (\text{A9})$$

The first FS torsion is

$$\begin{aligned} \tau_1 = & \left[\frac{1}{\kappa^2} \left(\kappa^4 - \dot{\kappa}^2 + \frac{r^2}{\Delta} \mathcal{H}^0 \right) \right. \\ & \left. - \left(a^2 + \frac{2a^2m}{r} + r^2 \right) (\mathcal{H}^1)^2 - \frac{4am}{r} \mathcal{H}^1 \mathcal{H}^2 - \left(1 - \frac{2m}{r} \right) (\mathcal{H}^2)^2 \right]^{1/2}. \end{aligned} \quad (\text{A10})$$

The explicit forms of $\Pi'(r)$, \mathcal{H}^0 , \mathcal{H}^1 , \mathcal{H}^2 , and their associated auxiliary functions are provided in the supplementary material.

Appendix A.2 Kerr–Schild Coordinates

For Kerr–Schild coordinates we define

$$\Delta_r \equiv 1 - \frac{2m}{r}, \quad (\text{A11})$$

$$\mathcal{A}_K \equiv a^2 + r^2, \quad (\text{A12})$$

$$\mathcal{Z}_K \equiv \mathcal{A}_K^2 - a^2(a^2 - 2mr + r^2). \quad (\text{A13})$$

The compact expression for the FS curvature scalar becomes

$$\begin{aligned} \kappa^2 = & -\Delta_r(\mathcal{R}^3)^2 - \frac{4am}{r}\mathcal{R}^3\mathcal{R}^1 + \frac{4m}{r}\mathcal{R}^3\mathcal{R}^2 \\ & + \left(1 + \frac{2m}{r}\right)(\mathcal{R}^2)^2. \end{aligned} \quad (\text{A14})$$

The first FS torsion is

$$\tau_1^2 = \frac{1}{\kappa^2} \left[\kappa^4 - \dot{\kappa}^2 - \Delta_r(B^0)^2 - \frac{4am}{r}B^0B^1 + \frac{4m}{r}B^0B^2 - \left(1 + \frac{2m}{r}\right)(B^2)^2 \right]. \quad (\text{A15})$$

The explicit expressions for \mathcal{R}^a , B^a , \mathcal{S}^a , and other auxiliary functions are provided in the supplementary material.

References

- [1] Hans Thirring. “Über die Wirkung rotierender ferner Massen in der Einsteinschen Gravitationstheorie.” In: *Physikalische Zeitschrift* 19 (Jan. 1918), p. 33.
- [2] Josef Lense and Hans Thirring. “Über den Einfluß der Eigenrotation der Zentralkörper auf die Bewegung der Planeten und Monde nach der Einsteinschen Gravitationstheorie”. In: *Physikalische Zeitschrift* 19 (Jan. 1918), p. 156.
- [3] L I Schiff. “Motion of a gyroscope according to Einstein’s theory of gravitation”. In: *Proc. Natl. Acad. Sci. U. S. A.* 46.6 (June 1960), pp. 871–882.
- [4] C. W. F. Everitt et al. “Gravity Probe B: Final Results of a Space Experiment to Test General Relativity”. In: *Phys. Rev. Lett.* 106 (22 2011), p. 221101. DOI: [10.1103/PhysRevLett.106.221101](https://doi.org/10.1103/PhysRevLett.106.221101). URL: <https://link.aps.org/doi/10.1103/PhysRevLett.106.221101>.
- [5] W. Rindler and V. Perlick. “Rotating frames in relativity”. In: *General Relativity and Gravitation* 22.11 (1990), pp. 1067–1081. DOI: [10.1007/BF00756329](https://doi.org/10.1007/BF00756329).
- [6] B. R. Iyer and C. V. Vishveshwara. “Frenet-Serret description of gyroscopic precession”. In: *Phys. Rev. D* 48 (12 1993), pp. 5706–5720. DOI: [10.1103/PhysRevD.48.5706](https://doi.org/10.1103/PhysRevD.48.5706). URL: <https://link.aps.org/doi/10.1103/PhysRevD.48.5706>.
- [7] O. Semerák. “Gyroscope on polar orbit in the Kerr field”. In: *General Relativity and Gravitation* 29.2 (1997), pp. 153–168. DOI: [10.1023/A:1018802203493](https://doi.org/10.1023/A:1018802203493).
- [8] Donato Bini et al. “The many faces of gravitoelectromagnetism”. In: *Classical and Quantum Gravity* 14 (1997), pp. 2584–2596. DOI: [10.1088/0264-9381/14/9/017](https://doi.org/10.1088/0264-9381/14/9/017).
- [9] O. Semerák. “Circular orbits in stationary axisymmetric spacetimes”. In: *General Relativity and Gravitation* 30.8 (1998), pp. 1203–1215. DOI: [10.1023/A:1018812325747](https://doi.org/10.1023/A:1018812325747).

- [10] K. Rajesh Nayak and C. V. Vishveshwara. “Gyroscopic Precession and Inertial Forces in Axially Symmetric Stationary Spacetimes”. In: *General Relativity and Gravitation* 30.4 (1998), pp. 593–615. DOI: [10.1023/A:1018870208493](https://doi.org/10.1023/A:1018870208493). eprint: [gr-qc/9808036](https://arxiv.org/abs/gr-qc/9808036).
- [11] O. Semerák. “Spin Precession Along Circular Orbits in Stationary Axially Symmetric Spacetimes”. In: *Monthly Notices of the Royal Astronomical Society* 308 (1999), pp. 863–875. DOI: [10.1046/j.1365-8711.1999.02791.x](https://doi.org/10.1046/j.1365-8711.1999.02791.x).
- [12] Kyriakos Destounis et al. “Extreme-mass-ratio inspirals into rotating boson stars: Nonintegrability, chaos, and transient resonances”. In: *Phys. Rev. D* 108 (8 Oct. 2023), p. 084062. DOI: [10.1103/PhysRevD.108.084062](https://doi.org/10.1103/PhysRevD.108.084062). URL: <https://link.aps.org/doi/10.1103/PhysRevD.108.084062>.
- [13] T. A. Apostolatos et al. “Spin-induced orbital precession and its modulation of the gravitational waveforms from merging binaries”. In: *Physical Review D* 49.12 (1994), pp. 6274–6297. DOI: [10.1103/PhysRevD.49.6274](https://doi.org/10.1103/PhysRevD.49.6274).
- [14] Mark Hannam et al. “General-relativistic precession in a black-hole binary”. In: *Nature* 610.7933 (2022), pp. 652–655. DOI: [10.1038/s41586-022-05212-z](https://doi.org/10.1038/s41586-022-05212-z).
- [15] Antoni Ramos-Buades et al. “SEOBNRv5PHM: Next generation of accurate and efficient multipolar precessing-spin effective-one-body waveforms for binary black holes”. In: *Physical Review D* 108.12 (2023), p. 124037. DOI: [10.1103/PhysRevD.108.124037](https://doi.org/10.1103/PhysRevD.108.124037). URL: <https://arxiv.org/abs/2303.18046>.
- [16] Héctor Estellés et al. “New twists in compact binary waveform modeling: A fast time-domain model for precession (IMRPhenomTPHM)”. In: *Physical Review D* 105.8 (2022), p. 084040. DOI: [10.1103/PhysRevD.105.084040](https://doi.org/10.1103/PhysRevD.105.084040). URL: <https://arxiv.org/abs/2105.05872>.
- [17] Simona J. Miller et al. “GW190521: Tracing imprints of spin-precession on the most massive black hole binary”. In: *Physical Review D* 109.2 (2024), p. 024024. DOI: [10.1103/PhysRevD.109.024024](https://doi.org/10.1103/PhysRevD.109.024024). URL: <https://arxiv.org/abs/2310.01544>.
- [18] N. V. Krishnendu et al. “Effect of double spin-precession and higher harmonics on spin-induced quadrupole moment measurements”. In: *Physical Review D* 109.2 (2024), p. 023016. DOI: [10.1103/PhysRevD.109.023016](https://doi.org/10.1103/PhysRevD.109.023016). URL: <https://arxiv.org/abs/2311.05506>.
- [19] Harsh Narola et al. “Gravitational-wave parameter estimation with relative binning: Inclusion of higher-order modes and precession, and applications to lensing and third-generation detectors”. In: *Physical Review D* 110.8 (2024), p. 084085. DOI: [10.1103/PhysRevD.110.084085](https://doi.org/10.1103/PhysRevD.110.084085). URL: <https://arxiv.org/abs/2507.10304>.
- [20] Leor Barack and Curt Cutler. “Using LISA extreme-mass-ratio inspiral sources to test off-Kerr deviations in the geometry of massive black holes”. In: *Physical Review D* 75 (2007), p. 042003. DOI: [10.1103/PhysRevD.75.042003](https://doi.org/10.1103/PhysRevD.75.042003).
- [21] Pablo F. Muguruza and Carlos F. Sopuerta. “Probing Kerr Symmetry Breaking with LISA Extreme-Mass-Ratio Inspirals”. In: *arXiv preprint* (2026). arXiv: [2604.06053](https://arxiv.org/abs/2604.06053) [gr-qc].
- [22] Paulami Majumder and K Rajesh Nayak. “Gyroscopic Precession in the vicinity of Static Blackhole’s Event Horizon”. In: *General Relativity and Gravitation* 55 (4 2023). DOI: [10.1007/s10714-023-03108-5](https://doi.org/10.1007/s10714-023-03108-5). URL: <https://doi.org/10.1007/s10714-023-03108-5>.

- [23] Paulami Majumder and K. Rajesh Nayak. “Gyroscopic precession in Reissner–Nordström spacetime”. In: *General Relativity and Gravitation* 57.4 (Apr. 2025), p. 63. ISSN: 1572-9532. DOI: [10.1007/s10714-025-03395-0](https://doi.org/10.1007/s10714-025-03395-0). URL: <https://doi.org/10.1007/s10714-025-03395-0>.
- [24] Roger Penrose. “Gravitational Collapse: the Role of General Relativity”. In: *Nuovo Cimento Rivista Serie 1* (Jan. 1969), p. 252.
- [25] Roy P. Kerr. “Gravitational Field of a Spinning Mass as an Example of Algebraically Special Metrics”. In: *Phys. Rev. Lett.* 11 (5 Sept. 1963), pp. 237–238. DOI: [10.1103/PhysRevLett.11.237](https://link.aps.org/doi/10.1103/PhysRevLett.11.237). URL: <https://link.aps.org/doi/10.1103/PhysRevLett.11.237>.
- [26] Piotr T. Chruściel et al. “Stationary Black Holes: Uniqueness and Beyond”. In: *Living Reviews in Relativity* 15.1 (May 2012), p. 7. DOI: [10.12942/lrr-2012-7](https://doi.org/10.12942/lrr-2012-7). URL: <https://doi.org/10.12942/lrr-2012-7>.
- [27] Charles W. Misner. “The Flatter Regions of Newman, Unti, and Tamburino’s Generalized Schwarzschild Space”. In: *Journal of Mathematical Physics* 4.7 (July 1963), pp. 924–937. DOI: [10.1063/1.1704019](https://pubs.aip.org/aip/jmp/article-pdf/4/7/924/19328324/924_1_online.pdf). eprint: https://pubs.aip.org/aip/jmp/article-pdf/4/7/924/19328324/924_1_online.pdf. URL: <https://doi.org/10.1063/1.1704019>.
- [28] Paul I. Jefremov et al. “Innermost stable circular orbits of spinning test particles in Schwarzschild and Kerr space-times”. In: *Phys. Rev. D* 91 (12 June 2015), p. 124030. DOI: [10.1103/PhysRevD.91.124030](https://link.aps.org/doi/10.1103/PhysRevD.91.124030). URL: <https://link.aps.org/doi/10.1103/PhysRevD.91.124030>.
- [29] Gabriel Andres Piovano. “Particles with precessing spin in Kerr spacetime: Analytic solutions for eccentric orbits and homoclinic motion near the equatorial plane”. In: *Phys. Rev. D* 113 (6 2026), p. 064024. DOI: [10.1103/jzbx-m1cp](https://link.aps.org/doi/10.1103/jzbx-m1cp). URL: <https://link.aps.org/doi/10.1103/jzbx-m1cp>.
- [30] Viktor Skoupý et al. “Spherical inspirals of spinning bodies into Kerr black holes”. In: *Phys. Rev. D* 112 (12 2025), p. 124054. DOI: [10.1103/x9yy-c2jq](https://link.aps.org/doi/10.1103/x9yy-c2jq). URL: <https://link.aps.org/doi/10.1103/x9yy-c2jq>.
- [31] Y. Chen et al. “Efficient simulations of high-spin black holes with a new gauge”. In: *Physical Review D* 104 (2021), p. 084046. DOI: [10.1103/PhysRevD.104.084046](https://doi.org/10.1103/PhysRevD.104.084046).
- [32] Maitraya K. Bhattacharyya et al. “Analytical and numerical treatment of perturbed black holes in horizon-penetrating coordinates”. In: *Phys. Rev. D* 102 (2 2020), p. 024039. DOI: [10.1103/PhysRevD.102.024039](https://link.aps.org/doi/10.1103/PhysRevD.102.024039). URL: <https://link.aps.org/doi/10.1103/PhysRevD.102.024039>.
- [33] Rohta Takahashi. “Horizon-penetrating transonic accretion discs around rotating black holes”. In: *Monthly Notices of the Royal Astronomical Society* 382.2 (2007), pp. 567–593. ISSN: 0035-8711. DOI: [10.1111/j.1365-2966.2007.11877.x](https://doi.org/10.1111/j.1365-2966.2007.11877.x). URL: <https://doi.org/10.1111/j.1365-2966.2007.11877.x>.